Chapter 5
IMAC 2025 Modal Expansion of Mixed-Domain Vibration Response Using Neuromorphic Event-based Imaging Data

Gabriella Gallegos, Tessa Lytle, Deborah Fowler, Fernando Moreu, Ryan Schultz, Chandler Smith, Timothy Walsh, and Tariq Khraishi

Abstract Obtaining comprehensive vibration response data is essential for characterizing structural response under vibration and shock environments. Full-field data acquisition methods such as digital image correlation provide valuable insight into structural response, however the computational resources and time required can be prohibitive in applications such as vibration control that require real-time insight. A common low-latency alternative is to expand vibration responses from accelerometer data at limited measurement points to full-field. However, channel count limitations can limit the spatial resolution of physical sensors and the corresponding frequency range of response the expansion procedure can accommodate. The emerging field of neuromorphic imaging presents a low-latency alternative to acquiring full-field vibration measurements, however the quality and confidence in the resulting data can vary based on factors such as displacement magnitude and feature geometry. In this work, the authors examine the combination of neuromorphic imaging and traditional modal-based expansion methods to achieve low-latency estimation of full-field responses with higher accuracy than either technique could independently achieve. A mixed-domain expansion approach is explored to combine displacement data collected using neuromorphic sending with accelerometer data. The investigation combines neuromorphic imaging data with accelerometer responses by evaluating sensor placement methods that complement both neuromorphic imaging and expansion and implementing the results in a mixed-domain expansion. The result of this research provides real-time response information for vibration control and other applications requiring low-latency dynamic response information.

Keywords Neuromorphic imaging · Expansion · Modal filter

Gabriella Gallegos
Graduate Student, Department of Civil, Construction, and Environmental Engineering, University of New Mexico, MSC01 1070, 1 University of New Mexico, Albuquerque, NM 87131, USA
e-mail: ggallegos6@unm.edu@unm.edu

Tessa Lytle
Graduate Student, Department of Mechanical Engineering, Worcester Polytechnic Institute, 100 Institute Rd, Worcester, MA 01609, USA
e-mail: tlytle@wpi.edu

Deborah Fowler · Ryan Schultz · Chandler Smith · Timothy Walsh
Sandia National Laboratories, 1515 Eubank Blvd. SE, Albuquerque, NM 87123, USA
e-mail: dfowler@sandia.gov; rschult@sandia.gov; chasmit@sandia.gov; tfwalsh@sandia.gov

Fernando Moreu
Assistant Professor, Department of Civil, Construction, and Environmental Engineering, University of New Mexico, MSC01 1070, 1 University of New Mexico, Albuquerque, NM 87131, USA
e-mail: fmoreu@unm.edu

Tariq Khraishi
Professor, Department of Mechanical Engineering, University of New Mexico, MSC01 1070, 1 University of New Mexico, Albuquerque, NM 87131, USA
e-mail: khraishi@unm.edu

Matthew Whelan et al. (eds.), *Dynamics of Civil Structures, Vol. 2*, Conference Proceedings
of the Society for Experimental Mechanics Series, https://doi.org/10.13052/97887-438-0147-4_5

Introduction

Acquiring comprehensive vibration response data is a critical capability for characterizing structural response under vibration and shock environments. Channel count limitations as well as mass loading effects can limit the spatial resolution of physical sensors such as accelerometers. Full-field measurements can be achieved using technologies such as laser doppler vibrometers (LDV) and digital image correlation (DIC), however both methods are prohibitively expensive and neither of these methods allow for real-time/low latency response insight which is critical for applications such as vibration control or digital twin capabilities. LDVs acquire response data one point at a time using a series of repeated tests. DIC acquires full-field data in a single test, however the extensive post-processing required to extract the relevant dynamic response information means the data cannot be used in real-time.

The emerging field of neuromorphic imaging applies computing techniques inspired by biological nervous systems to process and extract relevant data from image sensors in real-time for low-latency applications. Recent work [1] has used this technology to acquire full-field vibration measurements using digital video cameras. The unique component of neuromorphic cameras (also known as Dynamic Vision Sensors (DVS)) is that for each pixel, when a change in brightness exceeds a certain threshold, an event is triggered at the corresponding pixel location. The event stream is defined by the x and y coordinates, the brightness change indicated by either positive (+1) or negative (-1) polarity, and the time at each coordinate. This concept is illustrated in Figure 1 [18].

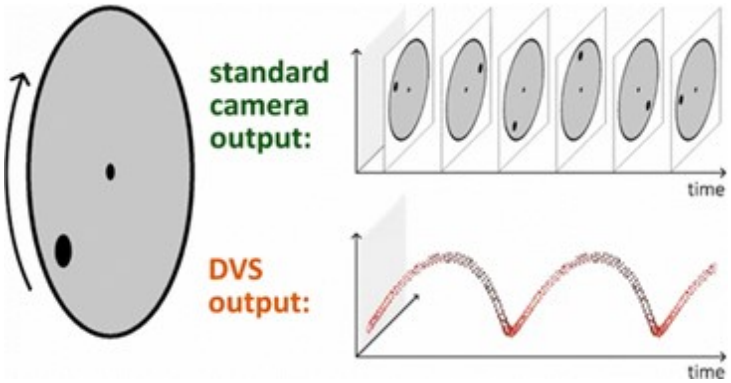

Fig. 1 Dynamic Vision Sensors (DVS) neuromorphic concept.

A popular low-latency alternative to full-field data acquisition is to expand vibration response from accelerometer data at limited measurement points. The most prevalent approach is modal expansion, where the full-field mode shapes derived from a finite element method (FEM) model are used to interpolate between the sensor measurements. Optimal placement of sensors is critical to successful implementation of these expansion procedures. Several approaches exist for optimizing sensor placement for expansion and other modal-filtering applications. These sensor selection methods seek to minimize the number of sensors while maintaining a well-conditioned inversion process. A poorly conditioned inversion will amplify noise and other data contaminants throughout the expansion process, producing poor interpolation results. Regularization methods have been explored as a viable approach to improve expansion results with a poorly-conditioned inversion [2]. However, tuning the regularization parameters is not a straight-forward process. Selecting an optimal degree of freedom (DOF) set is widely regarded as preferable when the test engineer has the ability to do so. Some cases may require both regularization and an optimized set of DOF. This occurs when channel count limitations prevent the ability to include enough DOF to allow for a well-conditioned inversion, or when the experimental data has a large amount of noise. Overall, DOF selection remains a pivotal component to successfully implementing expansion procedures, and various approaches exist to perform the DOF selection process.

Neuromorphic imaging and expansion procedures are both low-latency techniques to achieve full-field response information with different strengths and weaknesses. Expansion methods rely on pre-test analysis to select optimal DOF sets, and a finite element model of the system to generate the required mode shapes. Neuromorphic imaging is an emerging field. While full-field information is acquired, there are varying levels of fidelity and confidence in the results – response locations at points of high displacement and/or at feature edges have shown to be the most coherent, whereas points of low displacement may not result in practical response information. We speculate that combining neuromorphic imaging and model-based expansion could lead to improved low-latency estimation of full-field responses better than either technique could achieve independently. Neuromorphic imaging collects displacement data. Therefore, a mixed-domain expansion approach will need

to be implemented to integrate the neuromorphic displacement data with the accelerometer data. While fundamental expansion work utilizes data collected using a single measurement technique (such as accelerometers), recent work has developed methods to perform expansion using data collected across multiple domains, such as displacement and acceleration or strain and acceleration [3, 4].

The goal of this research is to investigate how to design a modal filter that integrates neuromorphic imaging data with accelerometer responses in a single expansion procedure by (1) evaluating DOF selection methods to place accelerometers in locations that complement the neuromorphic imaging data, and (2) implementing the resulting mixed-domain expansion. This investigation contributes to active areas of research in vibration measurements with neuromorphic imaging and mixed domain expansion procedures, and it will develop a foundation to explore other methods of fusing neuromorphic sensing and expansion techniques for an improved approach to acquire low-latency full-field response data. These methods could ultimately provide necessary real-time response information for vibration control, digital twin implementations, and any other applications requiring low-latency full-field dynamic response information.

Theory

The System Equivalent Reduction Expansion Process (SEREP) method is one of the most widely used modal expansion methods [5]. SEREP is performed in two steps. First, the responses are projected through a modal filter to estimate the modal coordinates (response of each individual mode), using

$$\mathrm{p(t)} = \mathrm{U_a}^{\mathrm{g}} \mathrm{x_a(t)} \tag{1}$$

where p is the matrix of the estimates of modal coordinates, U_a is the matrix of model mode shapes U partitioned to the reduced set of a DOF, and $x_a(t)$ is the matrix of time responses at a DOF. This modal filtering step is extremely powerful and used for a wide range of problems in modal analysis. The second step of the SEREP expansion procedure is the expansion step, where the estimates of modal coordinates are projected back into the physical domain using the full-field model mode shapes using

$$\mathrm{x_n(t)} = \mathrm{U_n p(t)} \tag{2}$$

where the subscript n is used to refer to the full set of model DOF and $x_n(t)$ is the matrix of experimental responses expanded to full field. SEREP expansion can also be used to expand experimental mode shapes, by using the set of test modes instead of $x_a(t)$. The success of the expansion procedure is dependent on two main challenges: choosing an appropriate set of mode shapes that can fully describe the dynamic response and choosing a set of DOF that can fully describe and differentiate between the mode shapes in the set. These two challenges are intricately linked – the number of mode shapes that can be included is limited by the amount of DOF/channel count available, and the more efficient the DOF set is the more mode shapes can be included for the same number of DOF. This project will focus on the second challenge, DOF selection, although evaluating whether the mode shape set is sufficient is always a necessary part of the process.

There are several popular approaches to DOF selection for modal filtering applications. Effective Independence was used for this work and compared to manually selecting a DOF set.

Effective Independence: Effective Independence [7] is a popular method for DOF selection that uses a computation of the fractional contribution of each sensor location to the linear independence of the mode shapes. At each step of the procedure, the independence distribution vector E_D is defined as the diagonal of the matrix E, using

$$E = \mathrm{U_a}\left[\mathrm{U_a}^T \mathrm{U_a}\right]^{-1} \mathrm{U_a}^T \tag{3}$$

where U_a is the matrix of mode shapes U partitioned to the reduced set of a DOF. Once computed, the minimum values of E_D are found and the associated DOF is removed from the candidate set. The procedure is repeated until the candidate set reaches the desired size.

Experimental Set Up

This investigation was conducted using a wing-shaped aluminum plate bolted to an aluminum block, with washers placed between the wing and the block. While the structure was relatively simple, complexities were introduced by the bolts and the non-symmetric design of the wing.

A finite element model of the structure was developed using Sierra/SD which can be seen in Figure 2b [19], consisting of an AL6061 block (16”x9”x3”) bolted to an AL6061 wing (13”x26”x3/16”). Various boundary conditions were explored, including fixed and a variety of spring supports, along with adjustments to material properties. Ultimately, free-free boundary conditions were applied, with point masses added to simulate the accelerometers. The model consisted of a hexahedral mesh with approximately 770,000 elements and required about 15 to 20 minutes to run. An experimental modal test was then conducted to compare the physical and calculated mode shapes, to ensure the accuracy of the model.

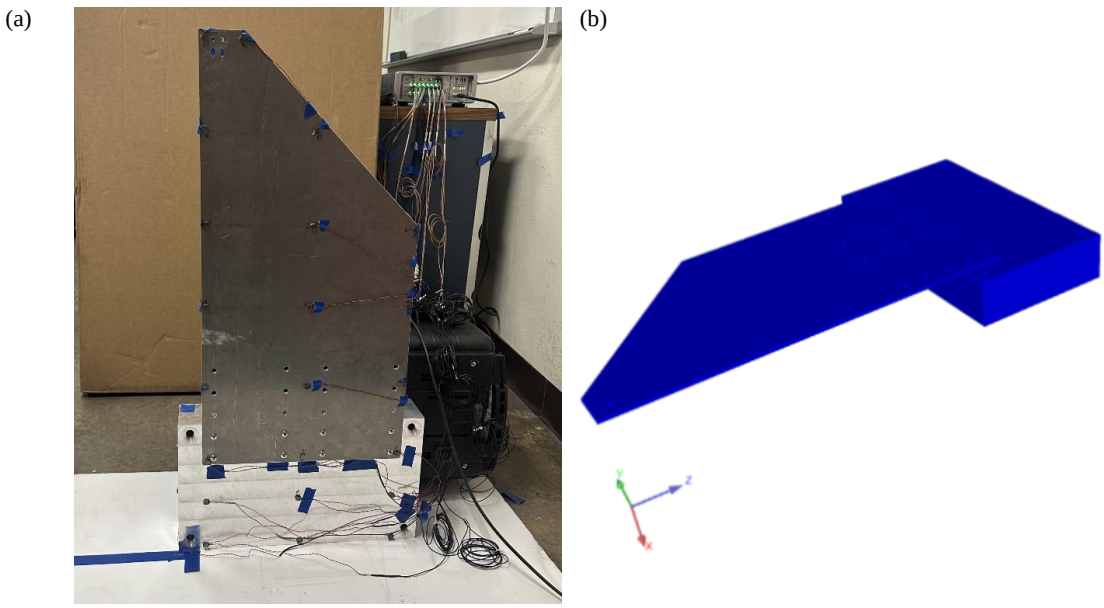

Fig. 2 (a) Experimental setup with 29 DOF. (b) FEM model free-free boundary conditions

An impact hammer test using Simcenter Testlab software [20] was conducted to measure the response at 24 locations, and the results were used to refine the FEM model. The 24 DOF were placed as 16 accelerometers on the wing and 8 accelerometers on the block. Accelerometers were placed on the wing to best capture the mode shapes, and the remaining accelerometers were placed on the block which was expected to have very minimal displacement. The structure was set upright with a thin foam poster board placed between the block and the concrete floor, as shown in Figure 2a. An acquisition time of 5 seconds was used to capture the bandwidth of interest, which was 819 Hz. A white plastic hammer tip was used to excite the desired frequency range of 0 to 600Hz. This frequency range was chosen to capture the first 10 modes. DOF 3 (as shown in Figure 9) was impacted a total of five times with the hammer.

The FRFs of the 24 accelerometers after an impact at DOF 3 are shown in Figure 3. The coherence was also checked, and throughout the entire frequency range of 0 to 600 Hz, there was no significant decrease, indicating that the collected results were of high quality.

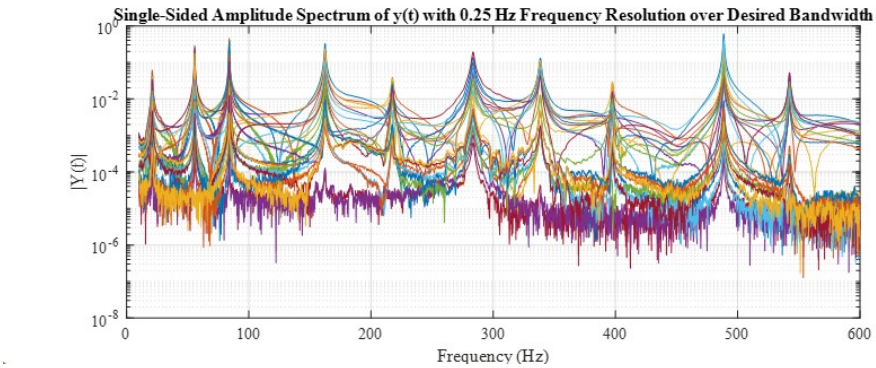

Fig. 3 Impact hammer test FRFs of the 24 accelerometers.

Impact Test Results

After ensuring the quality of the data collected from the impact hammer test, the data was processed using the Polymax curvefitter in Simcenter Testlab. Table 1 presents a comparison of the natural frequencies between the experimental and model natural frequencies.

Table 1 Comparison of Experimental and Model Frequencies for the First 10 Modes.

Mode #	Model (Hz)	Experimental (Hz)	% Error
1	25.5	20.8	22.5%
2	59.2	55.7	6.3%
3	89.0	83.9	6.1%
4	167.8	162.2	3.5%
5	223.9	217.2	2.7%
6	288.9	283.1	2.0%
7	341.4	338.4	0.9%
8	406.7	397.3	2.4%
9	496.3	488.7	1.6%
10	549.8	542.5	1.3%

Table 1 shows the most notable natural frequency discrepancies between lower value modes, particularly Mode 1. These discrepancies are attributed to difficulties in capturing the boundary conditions. A Modal Assurance Criterion (MAC) was used to compare the experimental mode shapes with the model mode shapes [11]. As shown in Figure 4, the MAC demonstrated a high correlation between the experimental and model mode shapes. Mode 1, which had the highest error in natural frequencies, showed a correlation of 0.94, while the remaining nine modes had correlations of 0.99 or higher. Figure 5 shows the comparison between the FEM results and experimental data for Mode 1. The FEM Mode 1 shows more movement along the block compared to the experimental Mode 1 which shows little to no movement along the block. This could indicate that the FEM free-free boundary conditions do not match the experimental boundary conditions of the block sitting upright on the floor.

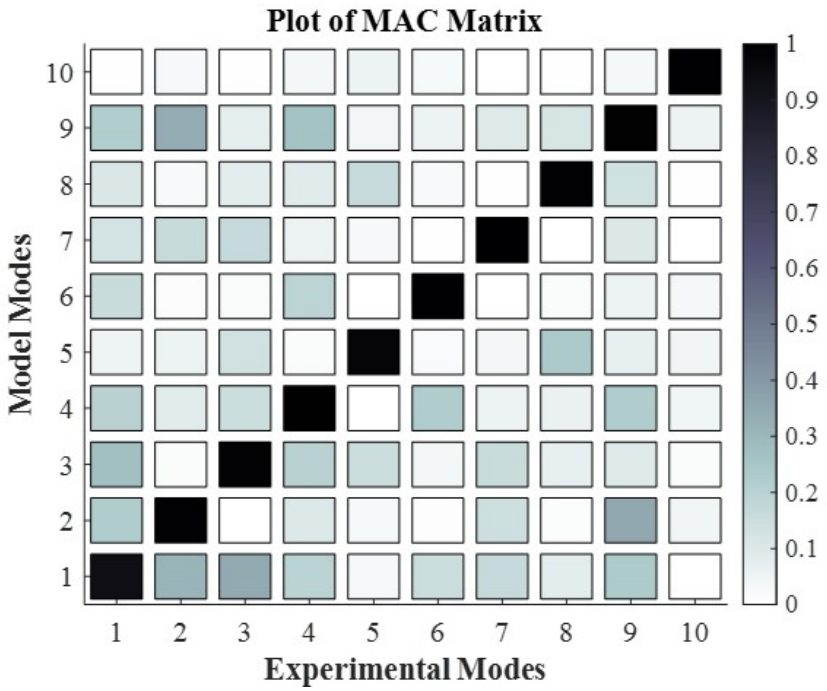

Fig. 4 MAC of experimental and model mode shapes.

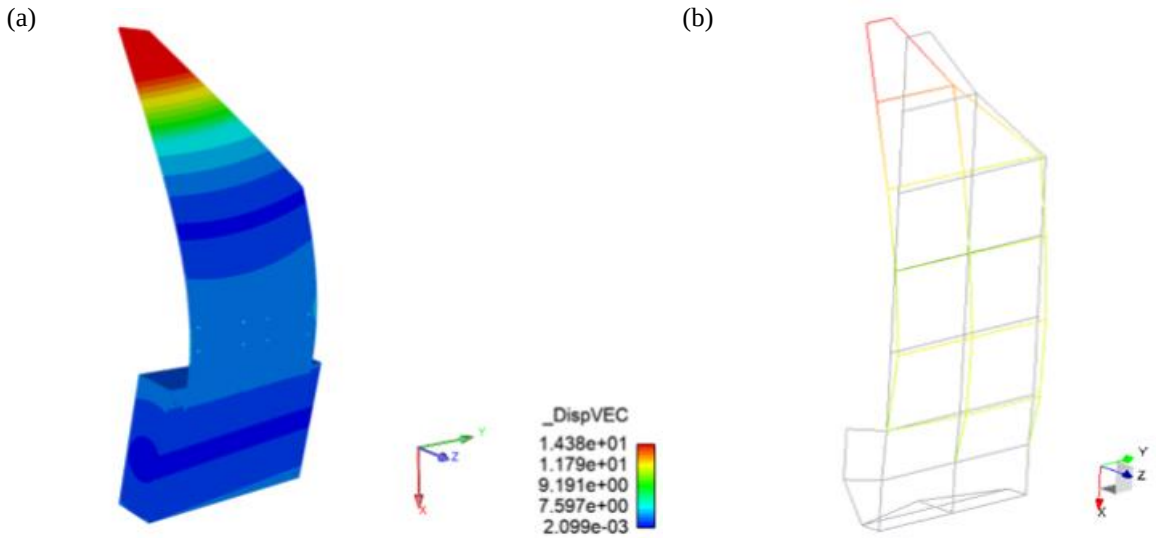

Fig. 5 (a) Experimental setup with 29 DOF. (b) FEM model free-free boundary conditions

Neuromorphic Imaging Testing

Neuromorphic imaging data was collected using a DVXplorer Mini camera with a spatial resolution of 640x480 pixels. The camera offers sub-1ms latency, 200μs temporal resolution, and can process up to 450 million events per second. The Dynamic Vision (DV) software used provides options such as event, accumulator, and capture blocks. All data is filtered by a Y-noise filter and a general noise filter before being output as a CSV file. The Y-noise filter removes flickering noise, while the general noise filter stores a map of event timestamps.

The first step was to calibrate the neuromorphic camera by determining the pixel-to-millimeter conversion factor. A 21x21 mm calibration square was taped to the tip of the wing and recorded at distances of two, three, and four inches. With the known spatial resolution of the camera and calibration square, the pixel-to-millimeter conversion factor was computed for the three measured distances. The results were then interpolated for distances from one to seven inches and plotted in Figure 6.

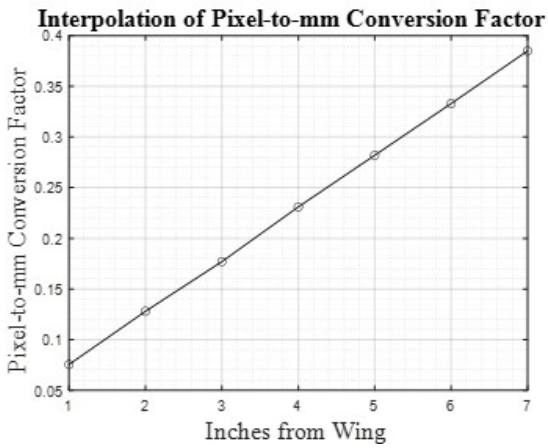

Fig. 6 Pixel-to-mm conversion factor interpolation.

The output of an event stream includes polarity, x and y coordinates, and a timestamp. The collected data is loaded into MATLAB and using the pixel-to-millimeter conversion factor, a specified region of interest is divided into 10x10 frames where events are clustered. The events are grouped into constant-sized clusters, and the average x-pixel values are computed for the specified region of interest. These average x-pixel values over time, combined with the conversion factor, are used to

calculate the displacement and plot the results. The plotted x-pixel values visualize the wing's movement. Figure 7 shows the comparison setup, where the camera was positioned 2 inches from DOF 1, and the LDV was aimed at DOF 1 while DOF 3 was impacted five times.

Fig. 7 Comparison setup with LDV and neuromorphic camera.

To ensure the code accurately captures the displacement, it was further fine-tuned by comparing the calculated displacement with measurements from the Laser Doppler Vibrometer (LDV). Figure 8 shows the comparison of the two methods, where it can be seen that the displacement is being captured.

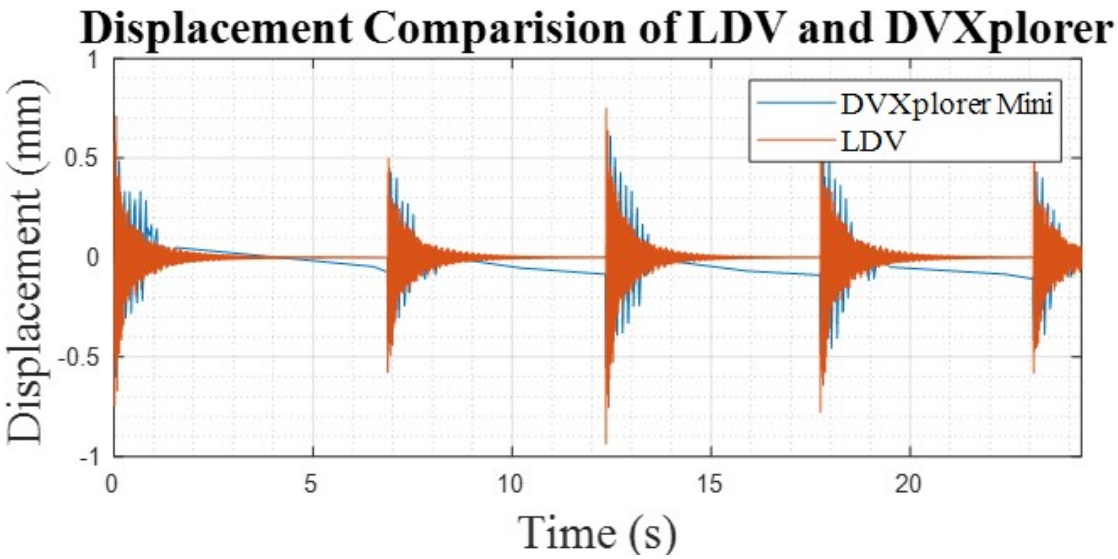

Fig. 8 LDV and DVXplorer Mini displacement comparison.

Neuromorphic imaging data was collected from three DOFs for this experiment: DOF 1, DOF 5, and DOF 7. For each DOF, the camera was placed at a distance of 1 inch from the wing, while an impact was applied at DOF 3. Figure 9a shows the experimental setup for DOF 1, and Figure 9b highlights the DOFs where the camera data was collected, including DOF 3, which was the impact DOF. These DOFs were chosen because they are located on the edges, making them accessible for the camera, and they are areas of high displacement, which allows the camera to record higher quality data.

Using the refined code and the collected data from DOF 1, DOF 5, and DOF 7, the displacement was collected and subsequently post processed. The data were first detrended and resampled into a uniform time vector using interpolation to ensure consistency in sampling. Due to the varying time steps of neuromorphic imaging data, a high sampling rate was used.

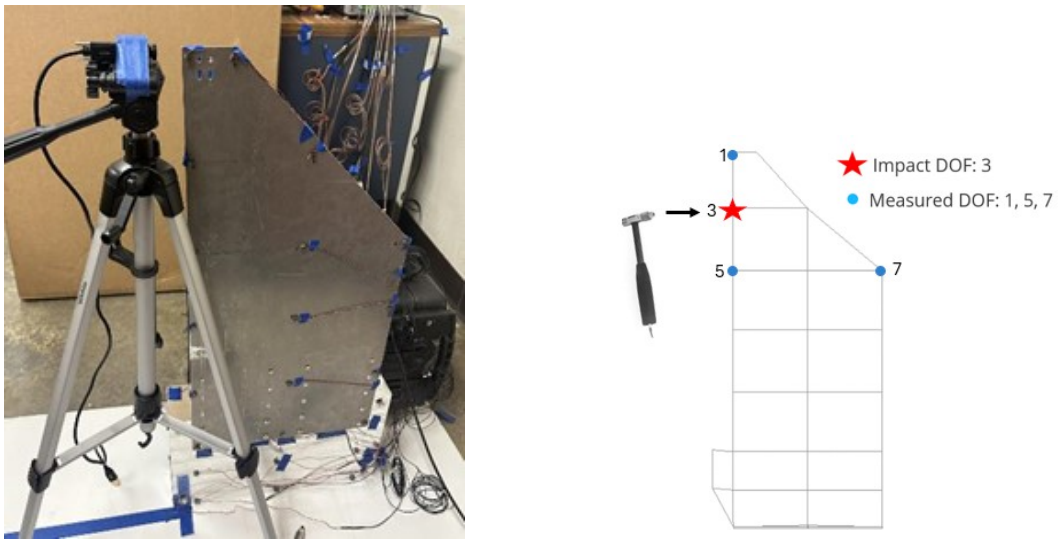

(a) (b)

Fig. 9 (a) Neuromorphic imaging data setup for DOF 1. (b) Layout of measured DOF and impact DOF.

A low-pass Butterworth filter was then applied to the resampled data to smooth out high-frequency noise and enhance signal clarity. The filtered displacement data were differentiated twice to obtain the acceleration time history, as shown in Figure 10. Additionally, the filtered displacement data were analyzed in the frequency domain using the Fast Fourier Transform (FFT), as seen in Figure 11. These steps collectively ensure that the data are clean, consistent, and ready for further analysis.

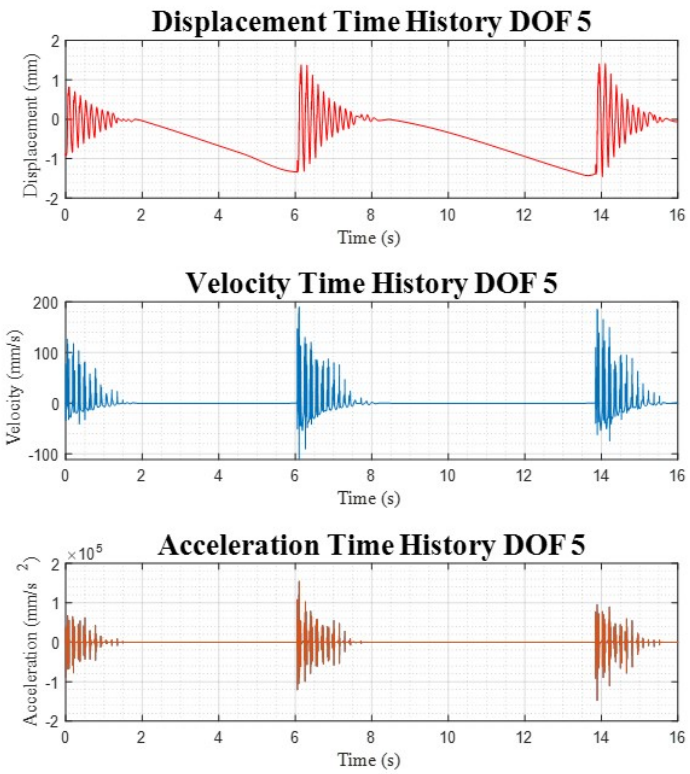

Fig. 10 Displacement, velocity and acceleration time history for DOF 5.

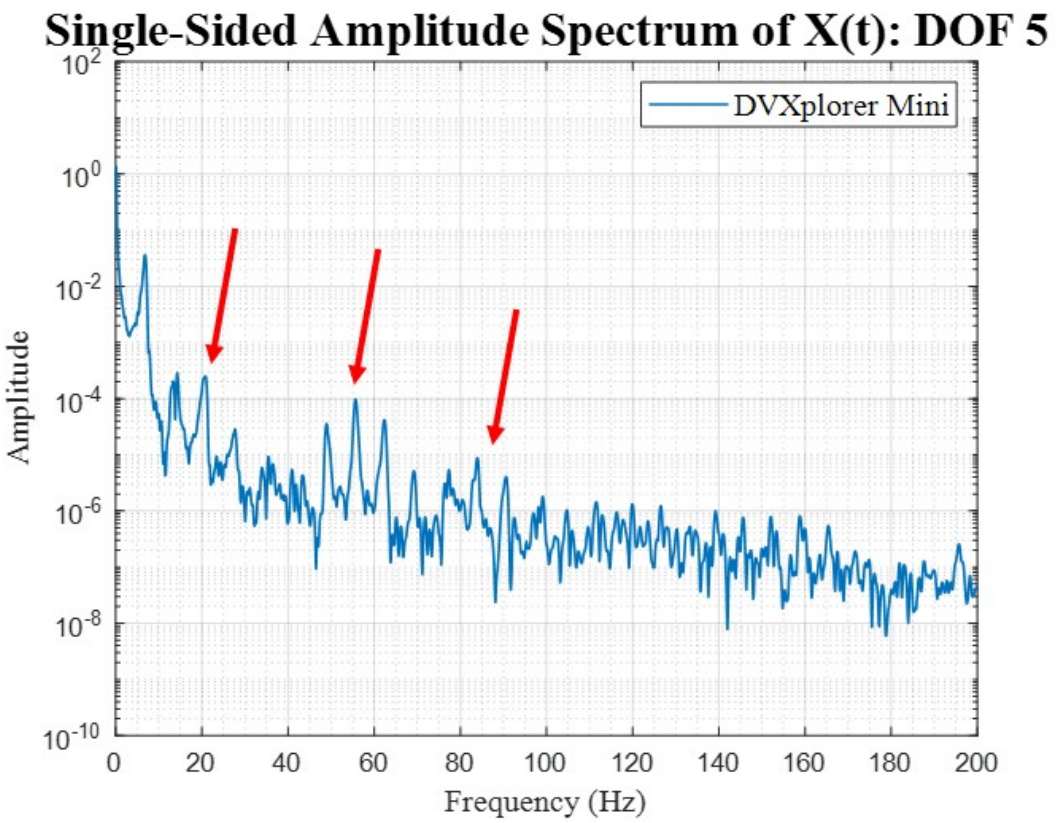

Fig. 11 FFT of DOF 5.

It is noted that the bandwidth of interest drops significantly after 200 Hz, no longer revealing clear peaks of natural frequency locations. For the continuation of the data processing, the focus is on the first three modes, all of which are within the first 100 Hz. Within the FFTs from the collected DOFs, the first three modes do appear as peaks despite the interference from other noise. This can be seen in Figure 11, where the first mode at 20.8 Hz, the second mode at 55.7 Hz, and the third mode at 83.9 Hz can be seen.

Degree Of Freedom Selection

The DOF (degrees of freedom) selection is critical for modal expansion because it determines which structural responses are captured. This selection impacts the accuracy of representing the structure's dynamic behaviors. In general, it is preferable to select the number of DOFs as 1.5 times the number of modes included in your finite element model. This ensures enough DOFs are selected to capture the structural response information of all of the selected modes. In this case, the finite element model included ten modes, so fifteen DOFs were chosen for the expansion. Two methods were explored for selecting the optimal DOF set, Effective Independence (EFI) and Condition Number Optimization.

Condition Number Optimization removed DOF 1, which is a key DOF where neuromorphic imaging data was collected, so this DOF set was not used for the mixed domain expansion. On the other hand, Effective Independence removed DOFs on the block, which did not interfere with the collected neuromorphic imaging data. To further explore the selection, a Manual Selection was also performed. This involved removing DOF 6, located in the middle of the wing, to evaluate how well the expansion would perform in an area with higher displacement, rather than focusing only on the block, which experienced very minimal displacement. The combination of using Effective Independence, as shown in Figure 12a, and manual selection, as shown in Figure 12b, ensured a more comprehensive and targeted comparison of DOF sets.

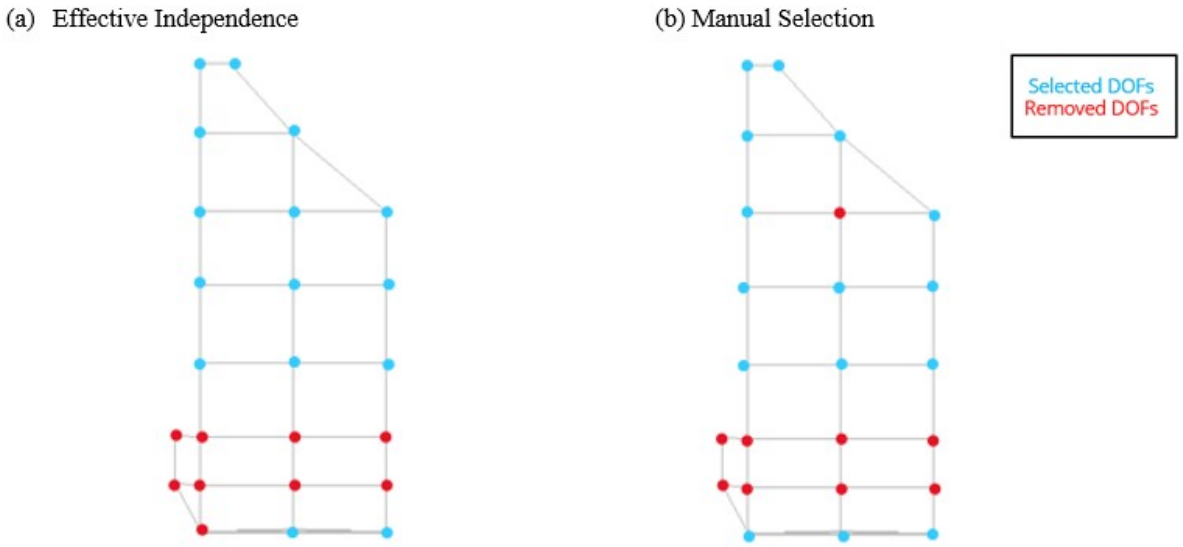

Fig. 12 DOF Selection Methods.

Results & Analysis

The System Equivalent Reduction Expansion Process (SEREP) was the modal expansion method utilized. This method was selected because it is one of the most widely used modal expansion methods. Referring to Equation 2, both single and mixed domain expansions using SEREP were then completed.

Where U_n is a mode shape matrix of all the DOF, U_a^+ is the pseudo-inverse of the mode shape matrix of the selected DOF from the model, and x_a is experimental acceleration response data of the selected DOFs (15 DOF x n frequency steps). The multiplication of U_n and U_a^+ acts as a modal filter, and x_n represents the estimated acceleration response data for all DOFs.

For single domain expansion, $x_{\ a}$ is composed of all the accelerometer data for the selected 15 DOFs.

$$x_a = \begin{bmatrix} Accelerometer\ DOF\ 1 \\ Accelerometer\ DOF\ 2 \\ Accelerometer\ DOF\ 3 \\ Accelerometer\ DOF\ 4 \\ Accelerometer\ DOF\ 5 \\ \vdots \\ Accelerometer\ DOF\ 15 \end{bmatrix}$$

In the mixed domain expansion, the accelerometer data for DOF 1, DOF 5, and DOF 7 were replaced with the post processed neuromorphic imaging data recorded at those DOF. Figure 13 is a reference showing the locations of DOF 1, DOF 5, and DOF 7.

$$\boldsymbol{x_a} = \begin{bmatrix} \boldsymbol{Neuromorphic}\ DOF\ 1 \\ Accelerometer\ DOF\ 2 \\ Accelerometer\ DOF\ 3 \\ Accelerometer\ DOF\ 4 \\ \boldsymbol{Neuromorphic}\ DOF\ 5 \\ \vdots \\ Accelerometer\ DOF\ 15 \end{bmatrix}$$

Using the DOF selected using the Effective Independence method, both a single and mixed domain expansion were completed. Figure 14 shows the comparison between the single domain expansion and the mixed domain expansion, specifically focusing on DOF 15. Figure 15 also references the location of DOF 15 and identifies the DOF set selected using the Effective Independence method. A Root Mean Square Error (RMSE) was then computed for the single and mixed domain expansion

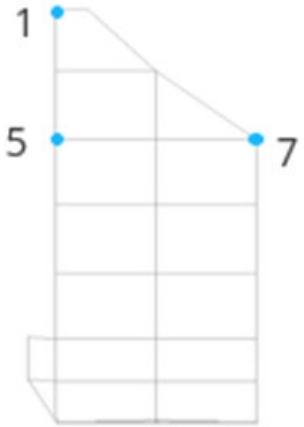

Fig. 13 DOF showing where neuromorphic imaging data was collected for the Mixed Domain Expansion.

estimates. The lower the RMSE, the better the estimation. For the single domain expansion, the RMSE was 0.024, while for the mixed domain expansion, it was 0.022. By computing the RMSE and examining the results, it is evident that the mixed domain expansion provides estimates for the block and represents the measured response data relatively well. This expansion was applied to DOFs which were located on the block. This could be useful in situations where it is difficult to instrument the base of the structure, especially if the base is less accessible.

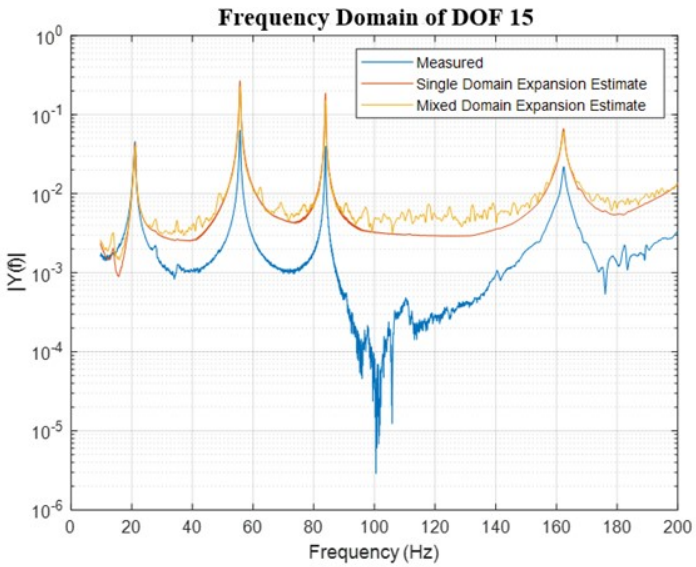

Fig. 14 Comparison of single and mixed domain expansion results for DOF 15 using DOF selected using Effective Independence.

Additionally, both single and mixed domain expansions were computed using DOFs selected from the Manual DOF selection method. Figure 16 shows the results of expanding to DOF 6, which was specifically chosen to assess how well the expansion performs in areas with higher displacement. For the single domain expansion, the RMSE was 0.013, while for the mixed domain expansion, it was 0.010. Although the mixed domain expansion estimate is noisier than the single domain expansion, it is evident that, despite the noise, the overall trend of the mixed domain expansion follows the measured data more closely than the single domain expansion. Figure 17 references the location of DOF 6 and identifies which DOFs were selected using the Manual DOF selection.

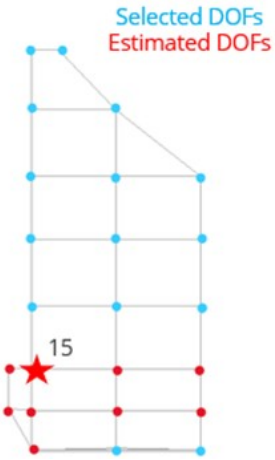

Fig. 15 Reference Image for DOF 15 and DOFs selected using the Effective Independence method.

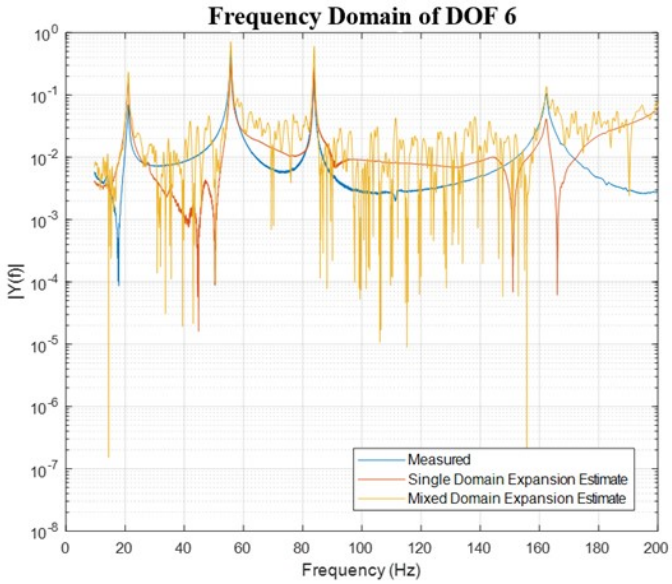

Fig. 16 Comparison of single and mixed domain expansion results for DOF 6 using DOF selected using the Manual DOF selection method.

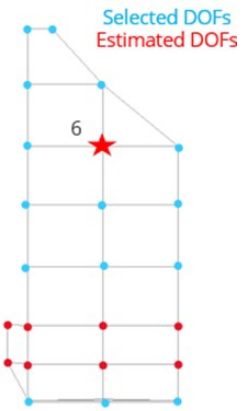

Fig. 17 Reference Image for Manual DOF selection and DOF 6.

Conclusion

From this research, three key conclusions have been drawn. Firstly, a mixed domain expansion can be achieved by combining neuromorphic imaging data with acceleration data. This conclusion is based on our results from applying the combined data to expand to different locations on the wing, yielding an RMSE comparable to that of a single-domain expansion. Second, a foundation for computing this new mixed domain expansion was developed by (1) collecting displacement from a neuromorphic camera, (2) exploring two DOF selection methods, and (3) converting neuromorphic imaging displacement to acceleration to compute a mixed domain SEREP expansion. Third, our results indicate that expanding to places of smaller displacement on the block produced less noisy estimates compared to expansions at points on the wing. This proof of concept lays the foundation for extending this technique, which can be applied to structures that cannot entirely use accelerometers due to, for example, their geometric complexity or their sensitivity to mass loading. It allows structural health monitoring in complicated structures where traditional methods could not be implemented.

These conclusions pave the way for additional areas of research. The first area for improvement is improving the collection and post-processing methods of the neuromorphic imaging data. While mixed-domain expansion is possible, it is limited by the frequency bandwidth capabilities of the camera, the resolution of displacement measurements, and the post-processing of the collected neuromorphic imaging data. Additionally, exploring experimental testing using different excitation methods, such as a shaker, or testing on a more flexible structure could produce better results. The neuromorphic imaging camera was detected as displacements, and a structure with either larger displacements or continuous excitation, rather than a single impact, would be more efficiently captured by the camera.

Acknowledgments This research was conducted at the 2024 Nonlinear Mechanics and Dynamics Research Institute hosted by Sandia National Laboratories and the University of New Mexico.

We would like to acknowledge and thank Bill Flynn and Charles Rice from Siemens for their support and for donating Testlab licenses throughout the summer.

Additionally, we would like to thank Rob Warmbold from Polytec for donating the lasers used for data collection during our experiments.

Sandia National Laboratories is a multi-mission laboratory managed and operated by National Technology & Engineering Solutions of Sandia, LLC (NTESS), a wholly owned subsidiary of Honeywell International Inc., for the U.S. Department of Energy's National Nuclear Security Administration (DOE/NNSA) under contract DE-NA0003525. This written work is authored by an employee of NTESS. The employee, not NTESS, owns the right, title and interest in and to the written work and is responsible for its contents. Any subjective views or opinions that might be expressed in the written work do not necessarily represent the views of the U.S. Government. The publisher acknowledges that the U.S. Government retains a non-exclusive, paid-up, irrevocable, world-wide license to publish or reproduce the published form of this written work or allow others to do so, for U.S. Government purposes. The DOE will provide public access to results of federally sponsored research in accordance with the DOE Public Access Plan. SAND2024-13539C.

References

1. C. Dorn et al., "Efficient full-field vibration measurements and operational modal analysis using neuromorphic event-based imaging," Journal of Engineering Mechanics, vol. 144, no. 7, p. 04018054, 2018.
2. C. Beale, R. Schultz, and D. Fowler, "Improved expansion results using regularized solutions," in Proc. 38th Int. Modal Analysis Conf., Houston, TX, 2020.
3. B. Daniels, A. Sabato, P. Avitabile, and R. Joshua, "Direct Expansion from Displacement to Strain Using Equivalent Transformation of Modal Coordinates," in Proc. 41st Int. Modal Analysis Conf. , Austin, TX, 2023.
4. J. Hower, R. Joshua, and T. Schoenherr, "A Method to Expand Sparse Set Acceleration Data to Full Set Strain Data," in Society for Experimental Mechanics Annual Conference and Exposition, 2023: Springer, pp. 23-42. '
5. J. O'Callahan, P. Avitabile, and R. Riemer, "System equivalent reduction expansion process (SEREP) " in Proc. 7th Int. Modal Analysis Conf., Las Vegas, NV, 1989.
6. A. Vince, "A framework for the greedy algorithm," Discrete Applied Mathematics, vol. 121, no. 1–3, pp. 247–260, 2002.
7. D. C. Kammer, "Sensor placement for on-orbit modal identification and correlation of large space structures," Journal of Guidance, Control, and Dynamics, vol. 14, no. 2, pp. 251–259, 1991.
8. A. K. Cline, C. B. Moler, G. W. Stewart, and J. H. Wilkinson, "An estimate for the condition number of a matrix," SIAM Journal on Numerical Analysis, vol. 16, no. 2, pp. 368–375, 1979.
9. B. C. Owens, R. L. Mayes, M. Khan, D. G. Tipton, and B. Zwink, "Flight Environments Demonstrator: Part I—Experiment Design and Test Planning," in Proc. 37th Int. Modal Analysis Conf., 2020.
10. R. J. Allemang, "A correlation coefficient for modal vector analysis," in Proc. of the 1st IMAC, 1982, pp. 110–116.
11. R. J. Allemang, "The modal assurance criterion–twenty years of use and abuse," Sound and vibration, vol. 37, no. 8, pp. 14–23, 2003.
12. "FEMtools$^{\mathrm{TM}}$ - Pretest and Correlation Analysis User's Guide, Version 3.7.0," Dynamic Design Solutions.

13. T. Schoenherr, “Using Modal Projection Error to Optimize Accelerometer Locations for a Modal Filter,” in Proc. 42nd Int. Modal Analysis Conf., Orlando, FL, 2024.
14. S. Joshi and S. Boyd, “Sensor selection via convex optimization,” IEEE Transactions on Signal Processing, vol. 57, no. 2, pp. 451–462, 2008.
15. Y. Saito et al., “Determinant-based fast greedy sensor selection algorithm,” IEEE Access, vol. 9, pp. 68535-68551, 2021.
16. D. P. Kouri et al., “Risk-Adaptive Experimental Design for High-Consequence Systems: LDRD Final Report,” Sandia National Lab.(SNL-NM), Albuquerque, NM (United States), 2021.
17. P. Avitabile, “Experimental modal analysis,” Sound and vibration, vol. 35, no. 1, pp. 20–31, 2001.
18. Gallego, G., Delbrück, T., Orchard, G., Bartolozzi, C., Taba, B., Censi, A., ..., & Scaramuzza, D. (2020). Event-based Vision: A Survey. IEEE Transactions on Pattern Analysis and Machine Intelligence, 44(1), 154–180.
19. Sierra, J. A., Underwood, O. D., Dewers, T. A., Stormont, J. C., & Cremer, G. A. (2022). Geomechanical Behavior of Cemented Granular Material for Wellbore Integrity. Sandia National Laboratories. https://doi.org/10.2172/1887938
20. Siemens Digital Industries Software. (n.d.). Simcenter Testlab. Siemens Community. Retrieved from https://community.sw.siemens.com/s/article/simcenter-testlab